A Preliminary Study on the Environmental Dependences of Avalanche Propagation in Silicon

Matthew W. Fishburn, *Member, IEEE*, and Edoardo Charbon, *Senior Member, IEEE*

***Abstract*—The growing use of single-photon avalanche diodes in strong magnetic fields has spurred an interest in understanding how the environment distorts the avalanche process. In this paper, we extend the multiplication-assisted diffusion avalanche model to include convection from a Lorentzian force caused by a strong magnetic field. Simulations imply that the avalanche is still expected to propagate at a speed of $2\sqrt{D/\tau}$, although from a point moving at a velocity given by the convection process. Simulations of quench time differences are compared to experimental results at multiple temperatures and magnetic fields. There is an absolute mismatch between simulations and experimental results of roughly 35%, although the simulations are able to predict the relative shift in quench times ranging from roughly 140 ps at -50 °C to 210 ps at $+50$ °C. As predicted by the models, no statistically significant shift is observed in avalanche quench time differences between magnetic fields at magnitudes of 0.1 and 9.4 T, regardless of orientation.**

***Index Terms*—Avalanche breakdown, avalanche propagation, Geiger-mode avalanche photodiode, single-photon avalanche diode (SPAD).**

I. Introduction

RECENT WORK in medical imaging has attempted to hybridize positron emission tomography (PET) and magnetic resonance imaging (MRI) systems. For example, combining the functional imaging capabilities of PET with MRI provides superior functional imaging in soft tissue. However, combining these two imaging techniques can be challenging as PET sensors may be sensitive to environmental factors required for MRI. Traditional PET sensors, such as photomultiplying tubes (PMTs), are known to be quite sensitive to magnetic fields.

Within the past decade, silicon photomultipliers (SiPMs) have been proposed as an alternative to PMTs. Based on arrays of single-photon avalanche diodes (SPADs), SiPM figures of merit show little to no dependence on the magnetic field. In this paper, we will examine, both numerically and experimentally, the avalanching process in a strong magnetic field, focusing on why the process is impervious to the field's effects.

Manuscript received October 14, 2012; revised October 18, 2012 and November 10, 2012; accepted January 15, 2013. The review of this paper was arranged by Editor A. Ionescu.

The authors are with the Delft University of Technology, 2628 CN Delft, The Netherlands (email: m.w.fishburn@tudelft.nl; e.charbon@tudelft.nl).

Color versions of one or more of the figures in this paper are available online at http://ieeexplore.ieee.org.

Digital Object Identifier 10.1109/TED.2013.2242469

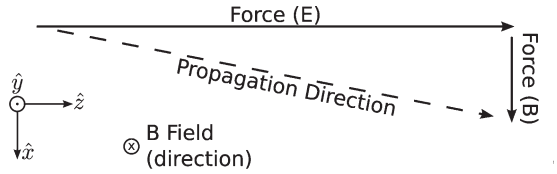

Fig. 1. Propagation velocity from forces in an avalanche diode.

II. Physics and Simulations

A multiplication-assisted diffusion process is known to cause avalanche propagation in silicon [1], which has been indirectly observed by electrical means [2] and directly with optical techniques [3]. However, the multiplication-assisted diffusion model does not account for forces originating from magnetic fields. In this section, this model will be extended to encompass convection forces from magnetic fields.

In silicon, saturation speed phenomena limit the maximum carrier speed, even at high-magnitude electric fields[4]. When additional forces act on a carrier, such as the Lorentz force generated by interactions with a static magnetic field, the carrier speed will remain saturated, but the propagation direction will shift slightly, as shown in Fig. 1. The assumption that $\vec{J} \propto \mu\vec{E}$, found in the derivation of the Hall coefficient, will not be valid due to the saturation speed phenomena. To calculate this shift, the forces from the electric field must be compared to the forces from the magnetic field. In an abrupt one-sided junction with a breakdown voltage of roughly 20 V, the peak electric field's magnitude is roughly $5 \cdot 10^5$ V/cm, implying that the average electric field in the multiplication region, the region with significant ionization, is larger than $4 \cdot 10^5$ V/cm [4]. Specifically, for a carrier with charge q in an electric field $4 \cdot 10^5$ V/cm $\hat{z}$, the force on the particle from the electric field is $\vec{F}_E = q\vec{E} = 6.4 \cdot 10^{-12}$ N $\hat{z}$.

Under a force of this magnitude, an electron is expected to accelerate to the saturation speed, roughly 10^5 m/s, in less than 20 fs. An electron moving at an average speed of $|v_s|$ in a 9.4-T magnetic field orthogonal to the direction of travel will create a force of magnitude $\vec{F}_B = q\vec{v} \times \vec{B} = 0.15 \cdot 10^{-12}$ N $\hat{x}$, although this assumes that $\vec{F}_B$ has a negligible effect on $\vec{v}$, an assumption which will be validated in a moment. Noting that $|\vec{F}_E|/|\vec{F}_B| \approx 40$, including the force from the magnetic field will modify $\vec{v}$ to be

$$\vec{v} = v_z\hat{z} + v_y\hat{y} + v_x\hat{x} \tag{1}$$

$$= \frac{|\vec{F}_E|}{\sqrt{|\vec{F}_E|^2 + |\vec{F}_B|^2}}|\vec{v}|\hat{z} + 0\hat{y} + \frac{|\vec{F}_B|}{\sqrt{|\vec{F}_E|^2 + |\vec{F}_B|^2}}|\vec{v}|\hat{x} \tag{2}$$

$$\approx 0.975|\vec{v}|\hat{z} + 0.025|\vec{v}|\hat{x} \tag{3}$$

with the planar component $v_x \approx 0.025 \cdot 10^5$ m/s ≈ 2.5 μm/ns.

Thus, including the magnetic field will cause less than a 2.5% change in the magnitude of the $\vec{v}$'s $\hat{z}$ component, and it is a reasonable assumption that this will not change the average force from the magnetic field. Also of note is that carriers will drift in a planar direction with a speed dependent on both the magnetic field strength and the electric field strength, with a direction dependent on both the carrier drift from the electric field and orientation of the magnetic field. As the electric field in an abrupt junction is not completely uniform, the velocity vector will vary as a function of the carrier depth. However, the avalanche dynamics are only distorted when the planar drift velocity acts on carriers within the region with high impact ionization, and because the ratio $|\vec{F}_B|/|\vec{F}_E|$ is roughly linear in this region, the velocity based on the average electric field will suffice for a first-order model.

In a multiplication-assisted diffusion model of avalanche spreading, the carrier concentration parallel to the electric field ($\hat{z}$-direction) is assumed to be uniform, so the carrier concentration $c(x, y, t)$ is a function of planar position and time. As long as carrier ionization shows no dependence on the magnetic field, which will be true for small shifts of direction for free carriers in silicon and small changes in the total force on free carriers, the addition of the Lorentz force will simply modify the carrier's direction. Under this assumption, the planar drift velocity is now identical to a convection velocity modifying the time-varying concentration, leading to a convection–diffusion equation [5]

$$\frac{\partial c}{\partial t} = D_{\text{eff}} \nabla^2 c - \vec{v}_c \cdot \nabla c + \frac{c}{\tau} + \Phi \tag{4}$$

where c is the spatially varying concentration, D_{eff} is the diffusion coefficient, $\vec{v}_c$ is the convection velocity vector, τ is a time constant governed by internal feedback processes, and Φ represents external processes that modify the carrier concentration (such as incident light). In practice, photon-starved conditions are assumed so that Φ can be set to zero and any incident photon-generated carriers are included in the solution's boundary conditions. As previously derived, $|\vec{v}_c| \approx |\vec{F}_B|/|\vec{F}_E| \cdot |v_s|$, with $\vec{v}_c$'s direction determined by the magnetic field's orientation.

A. Analytical Derivation of Spreading Speed

For a constant τ, $c(\vec{r}, t) = 0$ when $t < 0$, and $c(\vec{r}, 0) = \delta(\vec{r})$; the substitutions [6], $u(\vec{r}, t) = \exp(\gamma \cdot t + \vec{\lambda} \cdot \vec{r}) c(\vec{r}, t)$, $\vec{\lambda} = \vec{v}/2D$, and $\gamma = 1/\tau - |\vec{v}|^2/4D$ can be used to derive the analytical solution

$$c(\vec{r}, t) = \frac{\exp(t/\tau)}{4Dt} \exp\left(\frac{-|\vec{r} - t\vec{v}|^2}{4Dt}\right). \tag{5}$$

For a small threshold carrier threshold c_l, the outer edge of the avalanche at time t will be at position $\vec{r}$, implied to be

$$\begin{aligned} c_l &= \frac{\exp(t/\tau)}{4Dt} \exp\left(\frac{-|\vec{r} - t\vec{v}|^2}{4Dt}\right) \\ |\vec{r} - t\vec{v}| &= \sqrt{4Dt \cdot (t/\tau - \ln(4Dtc_l))} \\ |\vec{r} - t\vec{v}| &\approx t \cdot 2\sqrt{D/\tau} \end{aligned} \tag{6}$$

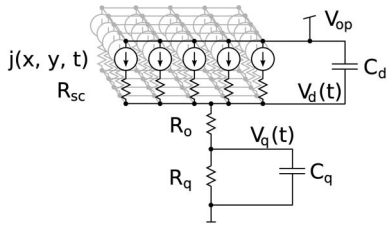

Fig. 2. Simplified finite-element method model of avalanche diode and quenching circuit.

implying that the avalanche is still expected to propagate with speed $2\sqrt{D/\tau}$ but will do so from a point that is moving at velocity $\vec{v}$. When $|\vec{v}| = 0$, the solution reduces to the solution given in [7], as expected.

B. Numerical Simulation

The τ term in (4) actually varies spatially due to nonuniformities in the breakdown voltage, and τ also depends on the local carrier concentration due to the space-charge phenomena. To work around these factors, numerical methods will be used to simulate solutions to the equation.

To simulate solutions to (4), a fourth-order Runge–Kutta method implementation tracks the carrier concentration c in an avalanche diode, along with the external capacitor state representing the avalanche diode's parasitic capacitance, sensing transistor capacitance, and routing capacitance. Fig. 2 shows a schematic representation of the simulated elements. Equation (4) governs the carrier concentration c in the diode, related to the current density by $j = qc|v|$. The τ term in (4) is calculated by finding the local voltage V_l based on the current flow caused by carriers across a space-charge resistor R_{sc} and using the time constant following the previously derived relations $\tau = 2(\overline{\alpha}(V_l) z_a - 1/\tau_a)$, $\tau_a = z_a/|\vec{v_s}|$, and $\overline{\alpha}(V_l) = A \cdot \exp(\sqrt{V_{\text{bd}}/V_l} \cdot \log(A/a))$, with z_a being the width of the multiplication region, assumed here to be 30% of the width of the depletion region, and constants A and a based on the material and the condition that $\overline{\alpha}(V_{\text{bd}}) = 1/z_d$ [4], [8].

The simulated spatial geometry is a 30 μm by 6 μm section of an avalanche diode that will be introduced shortly. The diode is split into 300 by 60 elementary diodes of size 100 by 100 nm^2, with the grid size set to be a fraction of the diffusion length of a free carrier during a time step. In order to capture a doping compensation effect from the guard ring's implants, V_{bd} is assumed to be temporally constant but varying in the planar directions. A spatially varying V_{bd} is approximated by finding the necessary implant diffusion of the well's carriers to match previously observed breakdown voltage shifts of diodes with differing geometries reported from the same chip [9]. Fig. 3 shows a contour plot of the spatially varying V_{bd}. A complete set of model parameters is shown in Table I.

When $t < 0$, $c = 0$ for all subdiodes. At time $t = 0$, an electron hole is assumed to be generated within one of the subdiodes, and the c at this particular subdiode is appropriately increased, while all other diodes at $t = 0$ have a concentration of zero. The transient current density and voltage waveforms will vary as a function of the trigger position. Fig. 4(a) shows the transient voltage observed by the quenching circuitry, V_q,

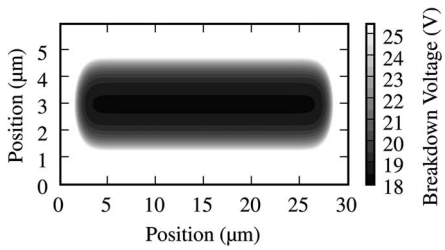

Fig. 3. Spatially simulated breakdown voltage (top view of diode).

TABLE I
MODEL PARAMETERS

Parameter	Value	Notes
V_{bd}	18.5-26.0V	See Fig. 3
V_{op}	20.9V	Free parameter
D_{eff}	$101 \cdot \exp(-.006 \cdot T)$ cm^2/s	[1], [7], [10]
$\lvert\vec{v}_s\rvert$	$1.9 \cdot 10^7/(1+.8 \cdot \exp(T/600))$ m/s	[11], [4]
T	223.15K to 323.15K (-50°C to +50°C)	Controlled variable
Element diode size	100 by 100 nm^2	[1]
$\vec{v}_c$	0, 2.5 μm/ns $\hat{x}$, 2.5 μm/ns $\hat{y}$	Based on b-fields
$c_p + c_d$	190 fF	Measured
c_d	40 fF	Calculated
R_o	700 Ω	Measured
R_q	1 MΩ	Simulated
R_{sc}	1.6 MΩ	Calculated

for edge- and center-seeded avalanches. The quench time, defined here as the time required for the quench voltage to rise from 100 mV to 2.0 V, can be extracted from the V_q waveforms, and Fig. 4(b) shows the quench time as a function of trigger location. Following convolution with a normal distribution, meant to signify the statistical nature of the ionization process, the quench time histogram can be extracted, as Fig. 4(c) shows. The normal curve in this procedure had a σ of approximately 40 ps, the value which minimizes the mismatch between the measured curve and a scaled version of the simulated curve.

As a result of the feedback processes in the avalanche, there is a smaller difference in quench times of edge- and center-triggered avalanches than expected. Avalanches triggered at the diode edge will cover a smaller area due to propagation in a single direction, implying that the excess bias will remain high, causing the propagation speed to remain high. As the propagation speed remains high, the edge-seeded avalanche spreads more rapidly than center-triggered avalanches, creating a smaller difference in quench time. Also, center-triggered avalanches quench at roughly the same time that the avalanche reaches the edge of the diode, creating smaller quench time differences in all avalanches seeded near the device center. Due to the second effect, the quench time histogram has a peak corresponding to center-seeded avalanches, with a relatively uniform count trailing. Of particular note is that, for avalanches uniformly spread throughout the diode, such as for a low-noise diode, the location of the initial peak can be used to extract the quench time for center-triggered avalanches. If additional events are triggered on the edge of the diode, the quench time difference can be used to indirectly estimate the avalanche propagation speed, or it can be used to observe the environmental effects on the avalanche propagation.

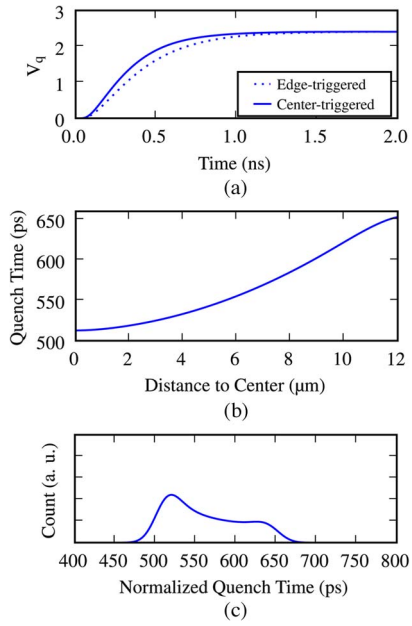

Fig. 4. **Quench time simulation**—(a) shows the simulated voltage observed by sensing circuitry for an avalanche initiated at $t = 0$. Extracting the time difference between when a V_q waveform reaches 0.1 and 2.0 V gives the quench time as a function of seed location, as (b) shows. Convolution of the quench time histogram with a normal distribution ($\sigma = 40$ ps) representing ionization noise yields the quench time histogram, shown in (c) with the initial peak normalized to 0 ps. (a) Simulated V_q after trigger at $t = 0$. (b) Quench time versus trigger location. (c) Quench time histogram.

These simulations were repeated for five temperatures and two orientations of magnetic field. Fig. 8 compares the expected quench times to observed values. In particular, the quench time shows less than a 5-ps difference for magnetic fields of magnitude less than 9.4 T. This is caused by the slow convection velocity and the quick quench time of the avalanche diode. Most of the diode-sourced current occurs within 500 ps of the onset, implying that the avalanche dynamics are completely unchanged because of the fast avalanche spreading. The simulations imply that the quench time at -50 °C should be roughly 2/3 the quench time at $+50$ °C.

III. EXPERIMENTAL SETUP AND RESULTS

This section describes an experimental setup capable of electrically measuring avalanche quench timing, indirectly allowing the measurement of avalanche propagation as described in the previous section.

In order to measure avalanche quench time differences and, thus, to indirectly measure avalanche propagation, specially designed SPADs with different quench timing as a function of seed position were fabricated in a 0.35-μm CMOS process. The SPAD design and chip architecture are identical to that published in [9]. The SPADs are a 24 μm by 6 μm rectangle capped by 6-μm-diameter semicircles. Three different metal coverings are used with these pill-shaped SPADS—one group of SPADs is left entirely uncovered, another is covered except for a 1-μm^2 hole near the edge, and the final group is covered except for a 1-μm^2 hole near the device middle. The SPADs are coupled via two comparators to an on-chip time-to-digital converter (TDC). The on-chip TDC uses a Vernier delay line

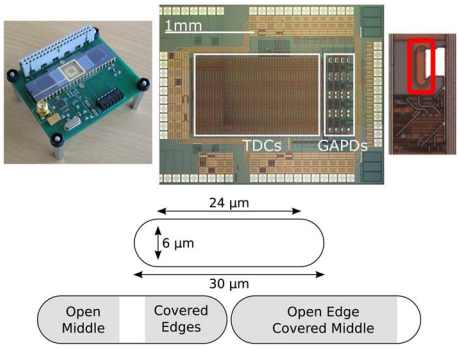

Fig. 5. (Top left) Daughterboard with SPADs, comparators, and two TDCs. (Top center) Micrograph of 0.35-μm CMOS IC, with a (top right) zoom of the edge-open pill-shaped SPAD, along with the (bottom) different structures.

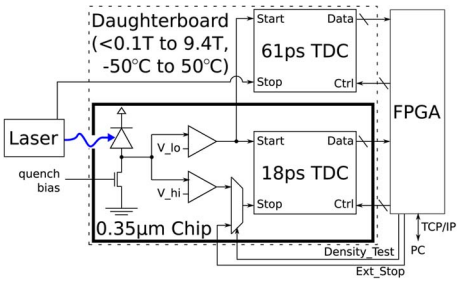

Fig. 6. System block diagram, after [12].

architecture, with an 18-ps resolution and a bias line allowing trimming for fabrication and environmental factors. A micrograph of the chip is shown in Fig. 5, along with an inset of a SPAD covered except for the edge. A selection line allows the TDC's STOP signal to be either an externally sourced periodic signal, useful for running a TDC density test, or the output signal from one of the SPAD-coupled comparators.

The SPADs are also coupled to an external high-range 70-ps-resolution TDC acquired from a commercial vendor. The on-chip TDCs are used to measure the avalanche quench time, whereas the off-chip TDC is used in jitter tests. The SPADs, two TDCs, and basic power circuitry are assembled together on a 6 by 7 cm^2 daughterboard, shown in Fig. 5. Extensive characterization data, including the characterization of an effect that reduces the active area to a roughly 24 μm by 2 μm rectangle, are reported in [9].

The two TDCs are coupled via parallel cables to an FPGA-based motherboard, which transfers the relevant TDC data to a computer workstation via a TCP/IP link. The motherboard and computer workstation contain components sensitive to strong magnetic fields and temperatures and must be kept at room temperature with a sub-100-mT field. Fig. 6 shows a block diagram of the complete measurement system.

When an avalanche is triggered in these diodes, the quench time of the voltage waveform varies because the avalanche propagates at a finite speed, causing current to flow more quickly through the diode when the diode is triggered closer to the center than at the edge. Measurements of the quench timing thus show whether the propagation speed increases or decreases with factors such as temperature or magnetic field, and results can be compared to simulations which estimate the propagation speed of the avalanche.

In order to measure the quench time difference between center- and edge-triggered avalanches as a function of environment, the daughterboard is placed inside either a temperature chamber or at various points in a small animal MRI system with an internal B-field of magnitude 9.4 T. The small animal MRI system is located in a temperature-controlled room with an ambient temperature of 25 °C, and hence, all measurements reported as a function of magnetic field are at this temperature. A TDC density test [13] is used to ensure that the TDC operated at identical resolutions irrespective of environment. The TDC does not require any trimming when operating inside of a 9.4-T magnetic field, although trimming is necessary as the ambient temperature changes. The applied voltage $V_{\rm op}$ is varied $+20$ mV/°C to keep a constant excess bias of 2.4 V on the diodes. The diode breakdown voltage in a 9.4-T field was observed to stay within 20 mV of a diode at sub-100-mT levels, and the applied voltage was not changed for tests at differing magnetic fields.

Fig. 7(a) shows avalanche quench times from an open-middle and an open-edge diode both in the dark and under light. Clearly evident from the subfigure, the quench times for edge- and center-triggered avalanches for these diodes vary by roughly 180 ps. The x-axis of all subfigures from Fig. 7 has been compensated, so the initial maximum of the dark count histogram is placed at a relative quench time of 0 ps. Fig. 7 was first presented in [12]; no new experimental information is presented in this paper, but the data are compared to the extended model. Because these bins have an average width of 20 ps, this maximum, which corresponds to the avalanche triggered in the diodes' centers, may be delayed or advanced by as much as 10 ps. Additionally, because the differential nonlinearity (DNL) of these TDCs is sizable, all counts are normalized to factor in the DNL of that particular TDC bin, acquired from the density test.

In order to acquire the quench time difference of edge- and center-triggered avalanches, the time of the dark count histogram's initial maximum can be compared to the time of the under-light histogram's maximum for edge-open SPADs. The initial maximum's time will correspond to center-triggered avalanches, and a Gaussian fit to the difference between the under-light and dark histograms will correspond to edge-triggered avalanches. Qualitatively, if the time difference between the fit's center and the initial maximum increases, then the avalanche has spread over a smaller area, implying that the avalanche propagates more slowly. Because the diffusion constant decreases and the time constant increases as the temperature increases, the avalanche should propagate more slowly for higher temperatures, implying that the quench time should increase with increasing temperature. This is exactly the behavior that Fig. 7(c) shows, with a quench time varying from roughly 140 to 220 ps as the temperature is increased from -50 °C to $+50$ °C.

Fig. 7(b) shows how the quench time varies when the diode is placed in a 9.4-T magnetic field that is either orthogonal to the minor or major axis of the diode. Note that the magnetic field direction is shown when looking from the top of the diode—in these p+/n-well diodes, electrons drift in a direction into the figure, and holes drift out of the figure. The diode

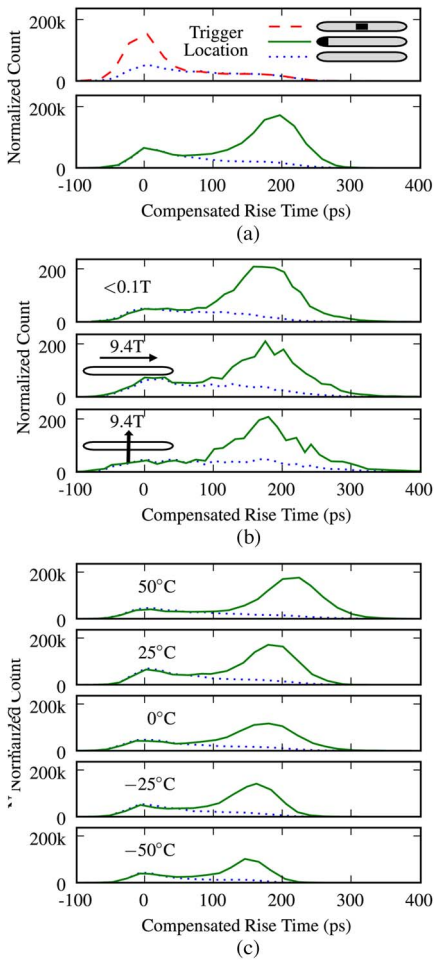

Fig. 7. **Quench times** are shown for differing (a) trigger positions, (b) magnetic fields, and (c) temperatures. The legend in (a) applies to all subfigures. After [12]. (a) Position sensitivity. (b) B-field dependence. (c) Temperature dependence.

trigger location is shaded on the pill shape in Fig. 7(a). There is no statistically significant shift in the avalanche propagation as a function of the tested magnetic fields. Due to the limited time available with the 9.4-T field, fewer samples were acquired in the density test used to characterize the TDCs in these conditions, and hence, the curves in Fig. 7(b) appear noisier.

The experimental setup has a major drawback, which is that the comparators might be dependent on the environment. In particular, the output timing dependence on the quench waveform slope is likely to change with the environment. Cadence Spectre [14] simulations carried out with data from the CMOS foundry implied that, in temperatures ranging from -50 °C to $+50$ °C, the comparators would have less than a 5-ps shift in the output start/stop signals for quench waveforms with rise times between 500 ps and 2 ns. No magnetic field simulation data are available.

Any comparator effects will also be mitigated by the differential nature of the measurements. If an environment-dependent distortion is present in both comparators, since both comparators measure the quench waveform, the first-order effect of this distortion is removed. If, however, a distortion is present in only one of the two comparators (for example, because one comparator is biased close to 0 V while the other is in the middle of the voltage range), the first-order effects of this distortion

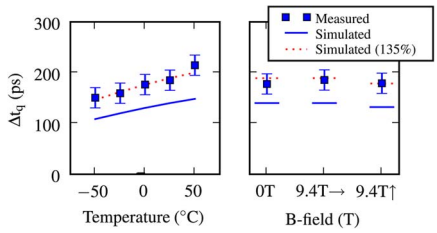

Fig. 8. Quench time difference is shown for various environmental conditions, and magnetic fields assume that the major pill axis is oriented horizontally ($\leftrightarrow$) and triggered on the left side.

would be canceled because the analysis uses relative quench times—the effect would exist in both the edge- and center-triggered avalanche quench times, and the relative quench time would not have the first-order effects of the distortion.

IV. Discussion

Fig. 8 summarizes the quench time variations Δt_q from Fig. 7 and compares these quench times to those predicted by the model. The aforementioned uncertainties are included in the experimental measurements as error bars. In general, the simulations predict a quench time that is 75% of the experimentally observed value. This is likely to be caused by several factors. First, the exact spatial distribution of $V_{\rm bd}$ is not known. Extracting $V_{\rm bd}$ heavily relies on implant processes, doping information, and annealing, none of which are readily available for most CMOS processes. Second, there are many first-order approximations which were assumed, such as how the time constant τ varies with the local voltage. Third, the effect of local charge variations was ignored. It has been shown that local charge variations are a second-order consideration compared to the multiplication-assisted diffusion process [7], although these processes are not negligible.

Despite the shift in expected quench time, the simulations are able to accurately predict the relative difference expected from different environments. The lack of a statistically significant result from shifting from a 0.1-T magnetic field to a 9.4-T one is important for working with avalanche diodes in strong magnetic fields. Even for long thin diodes operating at low excess biases, this is evidence that avalanche propagation itself is nearly impervious to strong magnetic fields. Coupled with evidence that neither the breakdown voltage nor the timing characteristics [15] show a dependence on the magnetic field, it is likely that avalanche diodes show no dependence on magnetic fields below 10 T. According to the model, avalanche propagation will exhibit little to no dependence on magnetic fields several times larger than 10 T, although this is predicated on the diode's breakdown voltage remaining constant under the strong magnetic fields.

Previous results have shown that the experimental timing jitter depends strongly on temperature but not on magnetic fields [15], [16]. Results imply a similar situation for avalanche propagation. Both the model and experimental results predict that the avalanche should propagate and quench more quickly as the temperature decreases. This is logical when considering that the diffusion coefficient D increases rapidly with temperature [10], while the fixed excess bias will cause τ to remain

relatively constant. As the propagation speed is $s = 2\sqrt{D/\tau}$, an increase in D will create a higher propagation speed and faster quenching.

Optical techniques are able to directly measure the avalanche propagation [3]. However, using optical techniques to measure avalanche propagation while in a 9.4-T field would impose considerable challenges. Current techniques require that the avalanche seed position be known to within roughly 1 μm, which would be difficult to achieve without a full microscope, and a TCSPC system capable of submicrometer resolution must be capable of measuring a device under the magnetic field. While such challenges are not insurmountable, the simplicity and compactness of electrical measurement techniques make observations in hostile conditions easier, although these techniques can only indirectly measure the avalanche propagation. Future work might address this problem by examining the mismatch between optical and electrical measurements of avalanche propagation in the same system or obtain more direct measurements of avalanche propagation itself.

A large shortcoming of the experimental setup is the inability to predict or measure any change in the behavior of avalanche propagation in a strong magnetic field. While the null result may seem uninteresting, it is important to scientists and engineers working with SPADs in the medical imaging field, particularly PET-MRI. Even with the geometry most likely to be affected by the field, no shift in performance should be expected.

As opposed to the null result predicted by an extended model and observed in a magnetic field, the multiplication-assisted diffusion model [1] successfully predicts a relative shift in the avalanche propagation as a function of temperature, a result which can be experimentally measured with the present setup. To the author's knowledge, no measurement of avalanche propagation as a function of temperature has been made; the multiplication-assisted diffusion model's correct prediction gives credibility to the model's ability to capture the physical essence of an avalanche.

V. Conclusion

Simulations using the previous model are able to predict the relative shift in quench times in temperatures ranging from roughly 140 ps at -50 °C to roughly 210 ps at $+50$ °C. The multiplication-assisted diffusion spreading model [1] has been extended to include convection from a Lorentzian force caused by a strong magnetic field. The modified model implies that the avalanche is still expected to propagate at a speed of $2\sqrt{D/\tau}$, although from a point moving at a velocity given by the convection process. As predicted by the modified model, no statistically significant quench time difference is observed between magnetic fields at 0.1 and 9.4 T, regardless of orientation.

Acknowledgment

The authors would like to thank F. Stuker and K. Dikaiou of ETH Zürich, along with Y. Maruyama of the Delft University of Technology, for their help with the present work. The authors would also like to thank Xilinx, Inc., and Acam Messelectronic GmbH for their hardware donations.

References

[1] A. Spinelli and A. Lacaita, "Physics and numerical simulation of single photon avalanche diodes," *IEEE Trans. Electron Devices*, vol. 44, no. 11, pp. 1931–1943, Nov. 1997.

[2] A. Lacaita, M. Mastrapasqua, M. Ghioni, and S. Vanoli, "Observation of avalanche propagation by multiplication assisted diffusion in p-n junctions," *Appl. Phys. Lett.*, vol. 57, no. 5, pp. 489–491, Jul. 1990.

[3] A. Ingargiola, M. Assanelli, I. Rech, A. Gulinatti, and M. Ghioni, "Avalanche current measurements in SPADs by means of hot-carrier luminescence," *IEEE Photon. Technol. Lett.*, vol. 23, no. 18, pp. 1319–1321, Sep. 2011.

[4] S. M. Sze, *Physics of Semiconductor Devices,* 2nd ed. New York: Wiley, 1981.

[5] R. F. Probstein, *Physicochemical Hydrodynamics,* 1st ed. Boston, MA: Butterworth, 1989.

[6] A. D. Polyanin, *Handbook of Linear Partial Differential Equations for Engineers and Scientists*. Boca Raton, FL: Chapman & Hall, 2001.

[7] A. Spinelli, "Limits to the timing performance of single-photon avalanche diodes," Ph.D. dissertation, Politecnico di Milano, Milano, Italy, 1995.

[8] A. Rochas, "Single photon avalanche diodes in CMOS technology," Ph.D. dissertation, École Polytech. Fédérale de Lausanne, Lausanne, Switzerland, 2003.

[9] M. Fishburn, Y. Maruyama, and E. Charbon, "Reduction of fixed-position noise in position-sensitive single-photon avalanche diodes," *IEEE Trans. Electron Devices*, vol. 58, no. 8, pp. 2354–2361, Aug. 2011.

[10] R. Brunetti, C. Jacoboni, F. Nava, L. Reggiani, G. Bosman, and R. J. J. Zijlstra, "Diffusion coefficient of electrons in silicon," *J. Appl. Phys.*, vol. 52, no. 11, pp. 6713–6722, Nov. 1981.

[11] C. Jacoboni, C. Canali, G. Ottaviani, and A. A. Quaranta, "A review of some charge transport properties of silicon," *Solid State Electron.*, vol. 20, no. 2, pp. 77–89, Feb. 1977.

[12] M. W. Fishburn and E. Charbon, "Environmental effects on photo-multiplication propagation in silicon," in *Proc. IEEE NSS/MIC*, 2011, pp. 572–574.

[13] B. Swann, B. Blalock, L. Clonts, D. Binkley, J. Rochelle, E. Breeding, and K. Baldwin, "A 100-ps time-resolution CMOS time-to-digital converter for positron emission tomography imaging applications," *IEEE J. Solid-State Circuits*, vol. 39, no. 11, pp. 1839–1852, Nov. 2004.

[14] *Spectre Circuit Simulator Reference*, Cadence, Berkshire, U.K, 2003.

[15] S. España, L. M. Fraile, J. L. Herraiz, J. M. Udías, M. Desco, and J. J. Vaquero, "Performance evaluation of SiPM photodetectors for PET imaging in the presence of magnetic fields," *Nucl. Instrum. Methods Phys. Res. A, Accel. Spectrom. Detect. Assoc. Equip.*, vol. 613, no. 2, pp. 308–316, 2010.

[16] S. Cova, A. Lacaita, M. Ghioni, G. Ripamonti, and T. A. Louis, "20-ps timing resolution with single-photon avalanche diodes," *Rev. Sci. Instrum.*, vol. 60, no. 6, pp. 1104–1110, Jun. 1989.

Matthew W. Fishburn (M'13) received the Ph.D. degree in electrical engineering from the Technical University of Delft, Delft, The Netherlands in 2012.

He is currently with the Delft University of Technology, Delft, The Netherlands.

Edoardo Charbon (SM'10) received the Ph.D. degree in electrical engineering and EECS from UC-Berkeley, Berkeley, California in 1995.

In Fall 2008, he has joined the Faculty of TU Delft, Delft, The Netherlands, as a Full Professor in VLSI design, succeeding Patrick Dewilde.